Synthesis, colloidal stability and unexpected selective lectin-binding properties of sophorose-functionalized iron oxide nanoparticles

Niki Baccile,[a,b,c,*] Florence Babonneau,[a,b,c] Romain Noiville,[a,b,c] Lorenzo Stievano,[d] Inge Van Bogaert[e]

a - UPMC Univ Paris 06, UMR 7574, Chimie de la Matière Condensée de Paris, F-75005, Paris, France

b - CNRS, UMR 7574, Chimie de la Matière Condensée de Paris, F-75005, Paris, France

c - Collège de France, UMR 7574, Chimie de la Matière Condensée de Paris, F-75005, Paris, France

d - Institut Charles Gerhardt Montpellier - AIME, UMR5253, Université Montpellier II, CC. 1502, Place E. Bataillon, F-34095, Montpellier cedex 5, France

e - InBio, Department of Biochemical and Microbial Technology, Faculty of Bioscience Engineering, Ghent University, Coupure Links 653, 9000, Ghent, Belgium

Abstract

Functional iron oxide nanoparticles (NP) have been synthesized in a one and two-step method using, for the first time, a natural functional glycolipid belonging to the family of sophorolipids (SL). According to the synthesis strategy, magnetic properties can eventually be tuned, thus putting in evidence the direct effect of the glycolipid on the final material's structure (maghemite and ferrihydrite). Here, we put in evidence the SL surface complexing properties on the metal oxide particles via its free COOH group as well as its interest as hydrophilic and stabilizing coating agent by mean of its carbohydrate moiety (sophorose). Most importantly, we have shown that the sophorose group is readily accessible to the outer layer of the nanoparticles by probing the specific interactions between the carbohydrate

functions and lectins, which are carbohydrate-binding proteins. Quite unexpectedly, but very interestingly, sophorose, an uncommon and poorly studied disaccharide, has shown a good selective affinity towards two non-sophorose-specific lectins, Concanavalin A (65% of ConA signal reduction found in this study with respect to 89% obtained on mannose-derived system under comparable conditions, where mannose is the classical Concanavalin A-targeting sugar) and lectin from *Bandeiraea simplicifolia* (BS-I). These results suggest that SL can be directly used as lectin-targeting compound in biomedical applications instead of chemically-engineered functional glycolipids.

Introduction

Multifunctional "smart" nanoparticles for biomedical applications constitute a domain of intense research where multiple materials and properties meet at the same time.[1] In this field, magnetic nanoparticles, and in particular iron oxide-based materials, occupy a special role because of their use in Magnetic Resonance Imaging (MRI) and magnetic hyperthermia applications.[2] Tailoring the surface chemistry of iron oxide nanoparticles allows to enhance and combine different properties, such as colloidal stability in aqueous environment, biocompatibility, low or non-existant toxicity, stealth effects towards physiological barriers (blood, liver, spleen, etc…) and cellular targeting, etc.[2a,c,3] To achieve part, or all, of these properties simultaneously, a surface multi-functional approach is generally employed, in addition to a more classical control of crystal structure and homogeneity, particle size distribution, shape, etc. Surfactants are generally used to improve colloidal stability in water because many nanoparticle syntheses are performed in organic media. Furthermore, neutral polymers such as polyethylene oxide or dextran are employed as stealth coating agents to pass physiological barriers, while proteins, enzymes, antibodies, or nucleotides are the most common cell targeting agents.[3,4] The success of such a multimolecular approach is demonstrated by the fact that some iron oxide nanoparticle systems have already been approved for clinical trials[2b,3,5] but their intrinsic complexity actually stimulates a research towards simpler nanosystems where the number of multifunctional surface agents is reduced to a minimum, if possible.

In recent works, several groups have developed an alternative strategy based on carbohydrate-functionalized nanoscale objects[6] combining the functions of selected nanomaterials (carriers, contrast agent, luminescent probe) with biocompatible sugars showing specific protein-targeting properties.[7] This new pathway is based on the use of well-designed glycolipids, or

glycoconjugates, compounds which have a desired sugar-based moiety covalently connected to an organic spacer. Penades *et al*. have used several techniques to coat gold nanoparticles and surfaces with functionalized glycolipids and to explore the carbohydrate-carbohydrate interactions tuning the nature of the sugar moiety.[6b] Specific interactions between magnetic nanoparticles and cancer cell lines were investigated by El-Boubbou *et al*.[6a] More complex sugar-functionalized silica-coated nanoparticles have been developed as well, where the silica serves as covalent binding layer through silane-based coupling agents (amide bonding, click-chemistry, etc…) between the nanoparticle and the carbohydrate-containing compound.[8] These works share some features: 1) glycoconjugates are specifically designed *ad-hoc*; 2) carbohydrates are known to bind specific proteins (lectins), for this reason the carbohydrate is chosen according to the desired targeting application; 3) the synthesis of the glyco-nanoparticles is composed of multiple steps where the glycoconjugate is synthesized first, then the nanoobject is made and finally functionalization is performed to build the glyco-nanomaterial. To this regard, different ways of grafting glycoconjugates have been tested: thiol-chemistry, amide coupling, click-chemistry, etc…

The "glyco" approach shows a number of advantages with respect to the multimolecular pathways discussed in the first paragraph. On one hand, tuning the end-chain functional group (thiol, carboxylic acid, amine, etc…) allows a larger variety of functionalizable surfaces; on the other hand, tuning the nature of the carbohydrate may influence solubility, biocompatibility and, for targeting applications, the specificity towards selected glucose-binding proteins.[7c] This last point is of paramount importance in the field of glycobiology, as carbohydrates are becoming very interesting tools to target cell lines according to the specific recognition between glycoproteins overexpressed at the surface of the cell themselves and the targeting sugar.[7b,d] Nevertheless, despite these indeniable advantages, the synthesis of glycoconjugates is somewhat tedious, time-consuming, expensive and unsustainable. For instance, several functional (thiol-derivatized) glycoconjugates of lactose, maltose and glucose reported by Barientos *et al*.[6b] can be obtained in no less than 5 steps, which involve, among others, highly toxic chemical compounds like azobisisobutyronitrile.

In this work we would like to promote the glycoconjugate strategy in combination with iron oxide nanoparticle functionalization by bringing it one step further: instead of using tailored, chemo-derived, glycolipids, we test sophorolipids (SL), which are biologically-derived glycoconjugates with a well-defined molecular structure. These compounds are synthesized by the yeast *Candida bombicola* and have been used so far for detergents[9] and skin care[10] applications. More recent anticancer,[11] antibacterial, self-assembly,[12,13] templating[12] and

metal-complexing properties[14] have been also put in evidence. SL, in their open acidic form, are composed of a sophorose unit (*i.e.* 2-*O*-β-D-glucopyranosyl-D-glucopyranose; β–Glc-(1-2)-Glc), attached to oleic acid through an ether bond on the C17 carbon atom of the fatty acid chain. This particular feature leaves the COOH group accessible. Hence, acidic SL are water-soluble, non-toxic, biocompatible and the COOH becomes an interesting functional, surface-binding, group. Sophorolipids are produced in large quantities from crops-based resources using a white biotechnology route, constituting a large advantage from an environmental point of view with respect to a chemical engineering approach.

In the field of microbially-derived glycoconjugates, few examples actually exist where specific glycolipids have been used as functional groups for nanoparticles. The main works were carried out by the group of Prasad where cobalt,[14b] silver[14a] and gold[15] nanoparticles were synthesized using the acidic form of sophorolipids. In particular, they have shown that sophorolipids are able to reduce metal salts (Ag, Au) *in-situ*[14a] and to stabilize the corresponding metal nanoparticles in water. Antibacterial and cytotoxic properties of sophorolipids-capped nanoparticles were also studied.

These works have the advantage of showing that sophorolipids can be successfully used as metal nanoparticle stabilizers but many questions are still open: can sophorolipids be employed in metal oxide nanoparticle synthesis? Can they be used in a one-step process? If so, is there any influence on the resulting metal oxide structure? Previous works were always carried out at very dilute sophorolipid and metal concentrations (10^{-3} - 10^{-4} M). Is it possible to work with more concentrated SL and metal salt solutions keeping a good colloidal dispersion in aqueous solutions? Is the sophorose group readily accessible and, if so, does it show any possible targeting property? The full answer to all these questions will undoubtedly open new perspectives for the use of microbial glycoconjugates as nanoparticle functional agents for biomedical applications. Nevertheless, one should keep in mind that the main drawback of working with microbial glycolipids is that, at the moment, controlling their molecular composition is not straightforward.

In this work, we show that acidic sophorolipids can be used as complexing agents in the synthesis of iron oxide nanoparticles (NP) in one and two-step syntheses. In particular, we use concentrated solutions of metal salts and SL ($5 \cdot 10^{-2}$ M) showing that stable colloidal solutions of iron oxide nanoparticles can easily be synthesized. We show that the choice of the synthesis method has a clear influence on the final metal oxide crystalline structure, on the magnetic properties and particle size distribution. Dynamic Light Scattering (DLS) experiments indicate that sophorolipids-derived nanoparticles exhibit an excellent colloidal

stability in water. Most importantly, we provide a direct proof of the accessibility of the sophorose group by mean of sophorose/lectin recognition experiments. Considering that sophorose is rare in nature and by far an uncommon disaccharide to be used in lectin-binding studies, this last point open very interesting and unexpected perspectives for the use of sophorolipids as potential cell targeting compounds. In particular, we show that sophorose-derived nanoparticles have an affinity for Concanavalin A, a typical mannose-binding protein. This unexpected feature shows that sophorolipids could potentially replace mannose-derived conjugates in drug delivery applications.[16]

Experimental

Synthesis of SL. Sophorolipids were produced by Candida bombicola ATCC 22214. The yeast was cultivated on medium as described before.[17] A fed-batch fermentation was run in a Biostat® B culture vessel (Sartorius-BBI Systems) with a maximum working volume of 1.5 L. Temperature (30 °C), pH (3.5), stirring rate (800 rpm) and airflow rate (1 vvm) were controlled by the Biostat® B control unit. 100 mL of an overnight grown shake flask culture was used to inoculate the fermentor. For maintaining a stable pH, appropriate amounts of 5 M NaOH were used. There was no correction for a too alkaline pH and fermentation started at pH 5.8 and was allowed to drop spontaneously till 3.5. Later unalterable incensement was seen as the end of the fermentation process. Feeding of rapeseed oil (Sigma) was started 48 hours after inoculation, and was adjusted to the consumption rate. Additional glucose (50 g/L) was added 150 hours after inoculation. Sophorolipids were extracted by the following procedure: 3 volumes of ethanol were added to the fermentation medium and yeast cells were removed by centrifugation. The water-ethanol mixture of the supernatants was removed under reduced pressure in a rotavapor. 2 volumes of ethanol were added to dissolve the sophorolipids and the residual hydrophobic carbon source. The mixture was passed over a Whatman filter to remove the water soluble components and ethanol was evaporated under reduced pressure in a rotavapor. Solid substances were dissolved in water (pH 6.5) and residual oil and fatty acid were extracted by an equal volume of hexane. The obtained sophorolipid mixture containing acidic and lactonic forms and di-, mono- and un-acetylated molecules, was hydrolysed with 5 M NaOH solution and extracted with pentanol according to procedure described in Ref. 18, giving rise to the un-acetylated acidic COOH form (17-L-([2'-O-β-D-glucopyranosyl-β-D-glucopyranosyl]-oxy)-octadecenoic acid). An average downfield 5 ppm shift from 172 ppm to 177 ppm in the ^{13}C NMR spectra of these compounds confirms the occurrence of the free COOH group.

Sample preparation. Iron oxide nanoparticles were synthesized using the co-precipitation method following a classical[19] procedure employed to obtain the inverse spinel structure typically observed in magnetite, where $[Fe^{2+}]/[Fe^{3+}]= 0.5$. According to the order of adding the reactants, we have tested two procedures in which the base is added either before or after mixing iron salts with SL. *One-step*: 0.177 g of $FeCl_3 \cdot 6H_2O$ were mixed with 0.108 g of $FeCl_2 \cdot 4H_2O$ in round-bottom flask containing 20 mL of MilliQ water and 0.409 g of the acidic form of sophorolipid. To this solution, about 2.7 mL of a 37 % ammonia solution was added under mechanical stirring. The system was kept under argon to limit oxidation and two temperatures were employed, room temperature (T= RT) and T= 80°C. These samples are referred to as, respectively, 1S-RT and 1S-80C. *Two-steps*: same as above but sophorolipids were added to the mixture only after addition of the ammonia solution and precipitation of the iron oxide nanoparticles. The samples are here referred to as 2S-RT and 2S-80C. In both cases, after one hour, the black precipitate was extracted by centrifugation and washed with water of MilliQ quality. This operation was repeated three times in order to completely eliminate any residual salts.

Sophorolipid-lectin interaction. Based on a previously published protocol,[6a] two different lectins were selected according to their respective affinity for sophorose. Fluorescein isothiocianate (FITC) conjugated Concanavalin A (ConA) and Lectin from *Bandeiraea simplicifolia* (BS-I) were purchased from Aldrich and used as such. For ConA, 3 mg of the lectin was dissolved in 30 mL of 10 mM HEPES buffer solution at pH= 7.4[20] using MilliQ water. For BS-I, 5 mg of the lectin are dissolved in 20mL of 10 mM HEPES buffer solution at pH= 7.4. Calibration of the lectin concentration was done on initial and diluted systems (dilutions: 1/2 and 1/10) by measuring the fluorescence emission spectroscopy at λ= 565 nm (excitation wavelength, λ_{ex}= 494 nm) of the FITC conjugated group. Three SL/nanoparticle systems were prepared by mixing a given amount of the 2S-80C sample with HEPES and these solutions were then mixed with the corresponding lectin buffers. The starting lectin concentration of the hybrid system composed of the lectin/nanoparticle/SL/buffer was 0.125 mg/mL and 0.05 mg/mL for, respectively, BS-I and ConA. As for the 2S-80C sample, three concentrations were explored: 0.5, 0.25 and 0.05 mg/mL.

DLS experiments. In experiments presented in Figure 5a-b, 30 µL of all samples solution obtained after synthesis were diluted in 1.5 mL of pure MilliQ water and water:ethanol=80:20 (vol:vol) mixtures. The solutions were filtered with a 0.20 µm filter before analysis. For the experiments shown in Figure 5c-d, 50, 100, 300, 500 mg of a washed

and dried maghemite powder, obtained from the two-step synthesis procedure described above without addition of SL, were mixed with 10 mL of MilliQ water to which 500 mg of sophorolipid were dissolved providing a resulting NP/SL mass ratio of 0.1, 0.3, 0.6, 1.0. In this last set of experiments, all solutions were analyzed at constant shutter opening diameter in the DLS apparatus.

Experimental techniques. Transmission Electron Microscopy was performed on a FEI Tecnai 120 Twin microscope operating at 120 kV and equipped with a high resolution Gatan Orius CCD 4k x 4k numeric camera. DigitalMicrograph™ software was used for image acquisition. Dynamic light scattering and zeta-potential measurements were run on a Malvern Zetasizer Nano ZS instrument (λ= 633 nm). UV-Vis adsorption experiments were run on a UVIKON-XL (Secomam) spectrometer using a wavelength scan mode while fluorescence emission spectroscopy was done on a FluoroMax-3 (Horiba Jobin Yvon) equipped with FluorEssence™ software and using a 10 mm quartz cell. Chemical analysis was obtained by energy dispersive X-ray spectroscopy (EDAX) using an Oxford X-Max (area: 20 mm2) detector installed on a Hitachi S3400N scanning electron microscope. Calibration of the instrument was performed on the Ti Kα at 4.509 keV. Data were obtained and averaged out after acquisition on at least four different sections of the sample distributed throughout the SEM support. Fourier-Transform Infra-Red (FT-IR) spectroscopy has been operated on a Perkin Elmer 400 spectrometer using the universal ATR sampling holder. The powder X-ray diffraction (XRD) study was performed on a Bruker D8 Advance diffractometer using Cu-Kα radiation (λ = 1.5418 Å) at 45 kV and 40 mA, 0.05° step size and 60 s per step over a 2θ range from 20° to 70°. ^{57}Fe Mössbauer spectra were measured with a ^{57}Co:Rh source. During the measurements, both the source and the absorber were kept at ambient temperature (294 K). The spectrometer was operated with a triangular velocity waveform, and a NaI scintillation detector was used for the detection of the gamma rays. The spectra of the measured materials were fitted to appropriate combination of Lorentzian profiles by least-squares methods using the program PC-Mos II.[21]In this way, spectral parameters such as the hyperfine magnetic field (B), quadrupole splitting and shift (Δ and ε, respectively), and isomer shift (δ) were determined. Isomer shifts are given relative to α-Fe metal.

Results and discussion

Materials structure. The co-precipitation method used to synthesize magnetic iron oxide nanoparticles (magnetite structure) is a well-established protocol that we could easily

reproduce in the two-step procedure, where sophorolipids were added only after the ammonia solution and nanoparticle precipitation.[19] The XRD diffraction pattern of the 2S-80C sample (Figure 1) shows the following d-values: 2.967, 2.527, 2.092, 1.714, 1.614, 1.478 Å, corresponding, respectively, to the (220), (311), (400), (422), (511), (440) Bragg diffraction planes of the iron oxide spinel cubic structure (JCPDS file, N° 19-0629). The magnetic nature of samples 2S-RT and 2S-80C can be easily evidenced by a simple external magnet, by which the powder grains are promptly attracted both in solution and in their dried form. The exact nature of the material structure (magnetite or maghemite) will be briefly discussed in the following paragraph.

On the contrary, the product 1S-80C, obtained from the one-step synthesis procedure, has a different XRD pattern, where only two peaks with very broad full-width at half maximum (FWHM) and corresponding to d-values= 2.527 and 1.478 Å are clearly visible. Such a XRD pattern is typical of 2-line ferrihydrite, $[Fe_5HO_8 \cdot (4H_2O)]$.[22] The corresponding materials synthesized at room temperature exhibit very similar XRD diffraction pattern for both procedures, indicating that temperature has no particular influence on the resulting crystal structure, contrary to the presence of sophorolipids in the reaction mixture. Differently from 2S-RT and 2S-80C, samples 1S-RT and 1S-80C are not attracted by an external magnet.

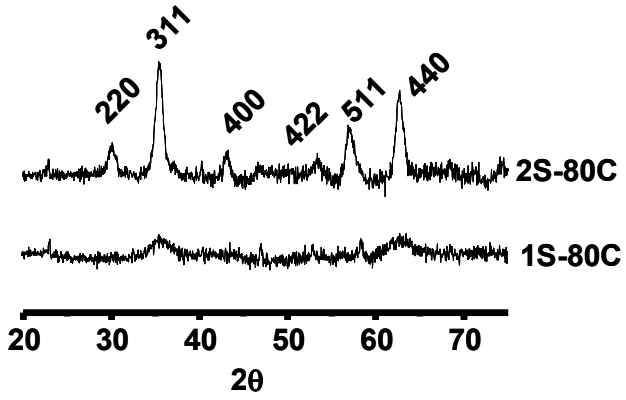

Figure 1 – X-ray diffraction pattern of the sophorolipid-containing iron oxide nanoparticles obtained at 80°C in the two-step (2S-80C) and one-step (1S-80C) synthesis processes. Reported values relate to the Miller (hkl) indices of the Bragg diffraction planes.

Additional information on the physico-chemical and magnetic nature of samples was obtained by ^{57}Fe Mössbauer spectroscopy. The room temperature Mössbauer spectrum of sample 2S-80C where the SL were added only after the precipitation of the iron oxide particles (Figure 2a, top), exhibits a relatively broad and asymmetric magnetic sextet centred at $\delta = 0.34(1)$ mm/s which can be fitted assuming a distribution of hyperfine magnetic fields (Figure 2b) and a very narrow quadrupole shift $\varepsilon = 0.01(1)$ mm/s. The strongest contribution

to the hyperfine field distribution is centred at a field of about 46 T. These values agree well with the presence of high spin trivalent iron in multiple octahedral and tetrahedral sites in maghemite (γ-Fe_2O_3),[23,24] which is derived from magnetite upon spontaneous oxidation of Fe^{2+} sites. The relatively low value of the maximum hyperfine field compared to literature values of well-crystallized maghemite together with the asymmetric shape of the Mössbauer profiles testify either from the finely divided nature of the maghemite particles which start to undergo superparamagnetic relaxation at room temperature, or for the presence of defects in the crystalline structure of the solid. The very slight difference in intensity observed between the corresponding lines of the spectrum at high and low velocity might be due to the presence of small amounts of magnetite in this sample.[23]

On the other hand, the room temperature Mössbauer spectrum of sample 1S-80C, where the oxide particles were precipitated in the presence of SL (Figure 2a, bottom) presents a relatively broad quadrupole doublet with an isomer shift $\delta = 0.36(1)$ mm/s and a quadrupole splitting $\Delta = 0{,}76(1)$ mm/s. Such parameters are typical of high spin trivalent iron, and agree well with the presence of superparamagnetic particles of ferrihydrite in this sample.

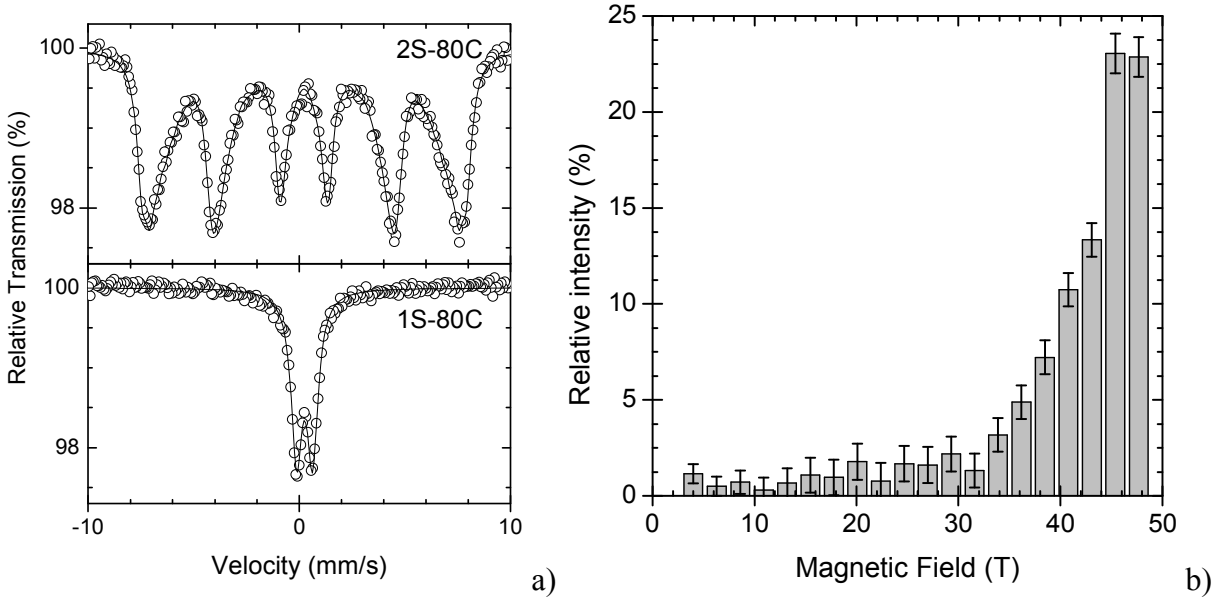

Figure 2 – a) Room temperature ^{57}Fe Mössbauer spectra of the sophorolipid-containing iron oxide nanoparticles obtained at T= 80°C in the two-step (2S-80C) and one-step (1S-80C) synthesis processes; b) Hyperfine magnetic field distribution obtained from the fit of the spectrum of sample 2S-80C.

TEM images and the corresponding particle size distributions are presented in Figure 3. All samples are composed of spherical nanoparticles whose size and homogeneity depend on the synthesis conditions. The two-step synthesis, 2S-80C and 2S-RT, provides particles whose average diameter is, respectively, 8.5 nm and 4.5 nm. As reported previously, the higher the

synthesis temperature, the larger the average particle size.[25] In both cases, the particle size distribution is comparable (± 2 nm) even if at room temperature bare particles as large as 12 nm can be observed. When SL is used since the beginning of the reaction, the particle size distribution of the final material is consistently different according to the temperature employed: at room temperature (Figure 3, sample 1S-RT), it is very broad, going from 3 to more than 20 nm while at T= 80°C the sample 1S-80C is composed of very small nanoparticles, with an average diameter of 2.8 ± 1 nm, if one disregards spurious aggregation on the TEM grid most likely due to the drying process.

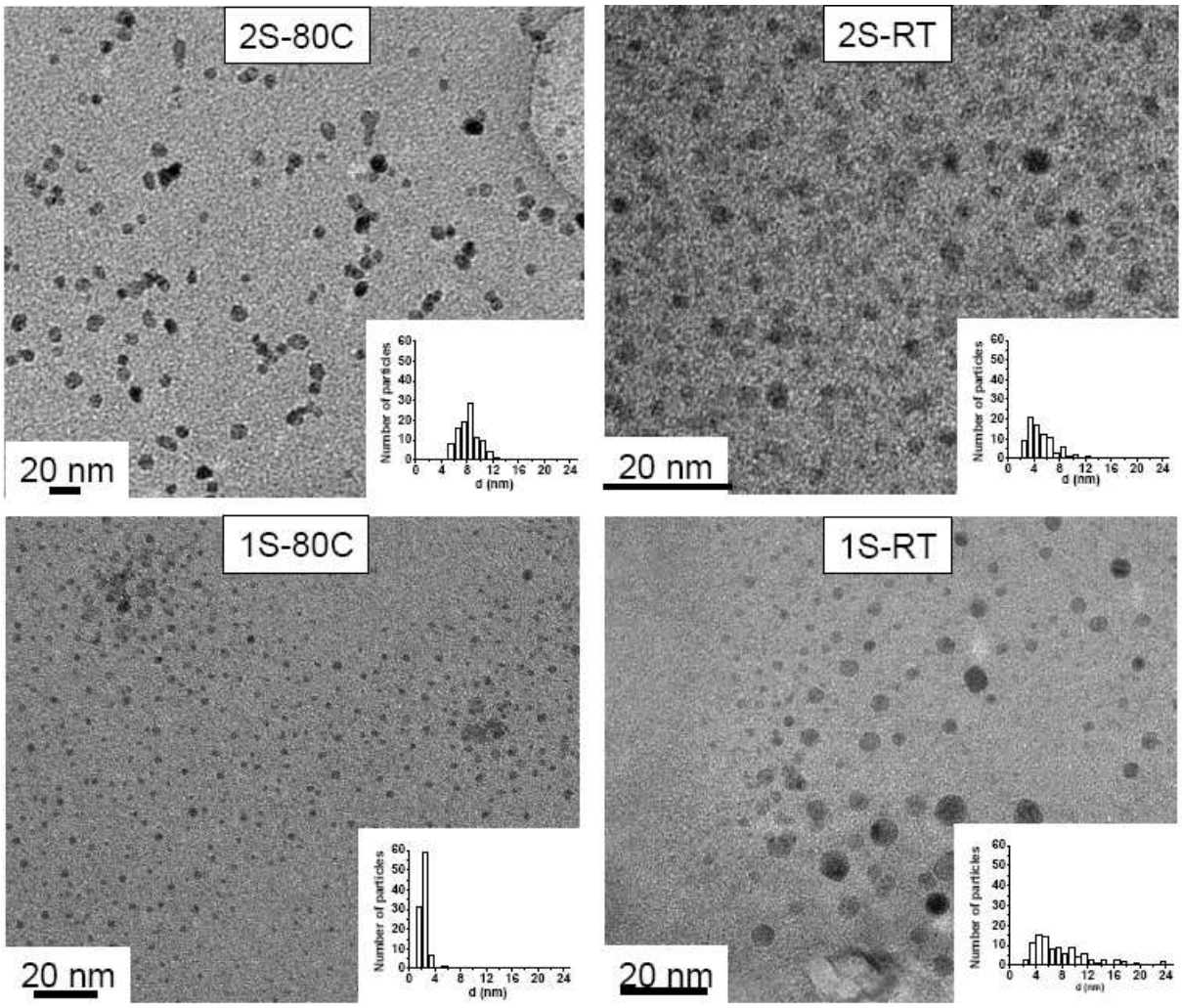

Figure 3 – TEM and particle size distribution obtained from TEM images of one-step and two-step, sophorolipid-containing, iron oxide nanoparticles.

As initially observed by XRD and Mössbauer spectroscopy, and finally confirmed by TEM experiments, one-step and two-step procedures provide sensibly different materials. Additional confirmations on the nature of the metal oxide particles in the different samples could be obtained by SEM/EDAX experiments, which allowed the quantitative analysis of the

elemental Fe/O ratio (Table 1). Interestingly, all one-step syntheses show a rather low Fe/O ratio (< 0.45) with respect to the two-step material (0.69 for 2S-80C). A comparison with the theoretical values provided in the same table confirms that the chemical composition of the one-step samples is very close to the theoretical Fe/O value expected for ferrihydrite. On the other hand, the value found for the two step samples agrees well with the dominant presence of γ-Fe_2O_3.

Table 1 – Experimental Fe/O ratio values obtained by SEM/EDAX for few selected materials obtained in the one-step and two-step synthesis. Theoretical Fe/O values for ferrihydrite and γ-Fe_2O_3 are also provided.

1S-RT	1S-80C	2S-80C	Ferrihydrite $Fe_5HO_8 \cdot (4H_2O)$[22]	γ-Fe_2O_3
0.43 ± 0.02	0.36 ± 0.13	0.69 ± 0.07	0.41	0.67

To better interpret such differences between one-step and two-step synthesis, one should consider that poorly ordered iron oxides are commonly obtained when iron salts are directly mixed with carboxylic acids, which are known to complex both Fe(II) and Fe(III) ions in water. For instance, in presence of citric acid, the kinetics of Fe(II) oxidation is largely reduced at specific amounts of COOH groups in solution (citrate/Fe(II) > 0.01). Similarly, it was shown that Fe(III) hydrolysis is retarded in presence of carboxylates.[26] In our synthesis procedure, the amount of COOH with respect to iron is comparable in terms of molar concentration, indicating that the promotion of poorly crystalline iron oxides is expected for one-step synthesis. Slower hydrolysis kinetic of both Fe(II) and Fe(III) retarded particle nucleation and inhibited growth of the nuclei,[27] which result in an uncontrolled stoichiometry within the final metal oxide. Reduction of the SL amount should prevent both uncontrolled metal complexation and formation of poorly crystalline iron oxides. Nevertheless, varying the SL/Fe ratio is not the purpose of this study.

Functionalization and colloidal stability.

FT-IR response of SL allow a better description of the nanoparticle functionalization. The FT-IR spectrum of pure acidic SL is shown in Figure 4 and it displays, among others, the following important resonances: =CH stretch (ν= 3004 cm^{-1}), SL aliphatic backbone (ν= 2920, 2850 cm^{-1}), C=O group in COOH (ν= 1705 cm^{-1}), C=O group in COO^- (ν= 1535, 1418 cm^{-1}), COH and CO in sophorose (ν= 1069, 1024 cm^{-1}). After synthesis, the sophorolipid shows the following features in the SL-functionalized iron oxide nanoparticles system:

- The presence of the symmetric and antisymmetric stretching bands of the aliphatic backbone (ν= 2920, 2850 cm^{-1}) shows that SL are still largely present on the nanoparticle surface, even after multiple washing steps. In addition, the absence of any X-ray diffraction pattern that can be attributed to SL (Figure 1) indicates that they do not crystallize at the nanoparticle surface after drying.

- The 3004 cm^{-1} resonance is detected. This peak is generally attributed to the =CH vibration of the oleic acid moiety. Its disappearance indicates that complexation on the nanoparticles can occur through the C=C double bond.[28] It was shown before that the C=C double bond is engaged in the complexation of SL-functionalized silver[14a] and cobalt[14b] nanoparticles. In the case of iron oxide nanoparticles, this mechanism does not seem to be the case, at least for the samples prepared at room temperature while that may occur for the high-temperature derived samples, where this resonance is difficult to see.

- The COOH functional group (ν= 1705 cm^{-1}) is largely reduced in intensity while two resonances, ν= 1535, 1418 cm^{-1}, mark the presence of COO^- (asymmetric stretching - ν_{as} - and symmetric stretching - ν_s - vibrations, respectively). This behaviour is attributed to the complexation of the iron oxide surface by the carboxylate group of the sophorolipid and is in agreement with the synthesis conditions. It was established before that the difference, $\Delta = (\nu_{as} - \nu_s)$, can be related to the way carboxylates bind to the metal oxide surface. For $\Delta > 200$ cm^{-1}, a monodentate binding occurs; for $\Delta < 110$ cm^{-1}, a bidentate binding takes place while for $140 < \Delta < 200$ cm^{-1}, a bridging mechanism best describes the carboxylate-metal coordination. One should nonetheless observe that data obtained from such a simple calculation are qualitative because of the presence of the CH bending at about 1436 cm^{-1}, which may overlap with COO^- stretching resonance, hence inducing an erroneous attribution of this peak. In our materials, we find that $\Delta \sim 130$ cm^{-1} for both one-step derived samples, suggesting a possible bridging coordination mode, while it decreases to $\Delta \sim 115$ cm^{-1} for both two-step derived samples, indicating a possible bidentate binding instead,[29] even if coexistence of both mechanisms should not be excluded.

- The COH groups of the sophorose head, whose resonances are detected in the region between 1160 and 750 cm^{-1}, might also be involved in the complexation of the iron oxide surface, as already described for similar systems.[30] The 1070 and 1020 cm^{-1} bands, attributed to a C-O stretching coupled with C-C stretching and O-H deformation, do not display any significant shift throughout all samples-set. This is also the case for the resonance at 1160 cm^{-1} (C-O-C glucosidic linkage stretch coupled with C-OH stretch and OH deformation),

exception made for the 1S-80C sample, whose broadening seems quite obvious. Even if these data indicate that, for most samples, sophorose is probably not involved into hydrogen bonding with the iron oxide surface, a competing complexation mechanisms of iron by COH groups should not be excluded, as largely discussed by Weissenborn et al.[30] The region below 1000 cm^{-1}, where carbohydrate ring vibration (ν= 935, 710 cm^{-1}), breathing modes (ν= 765 cm^{-1}) and C_1H deformation (where C_1 is the anomeric carbon of sophorose) appear (equatorial C_1H deformation: ν= 850 cm^{-1}; axial C_1H deformation: ν= 890 cm^{-1}) are typically observed to put in evidence any eventual complexation mechanism. The band at ν= 890 cm^{-1}, which appears in both pure and adsorbed SL, is related to the axial C_1H deformation of the β-D-glucose units.[31] In case of conformational changes, which were described for carbohydrate-complexed iron oxide systems,[30] this band is expected to shift by at least 40 cm^{-1}, which is not the case here for none of the samples, suggesting that complexation of surface iron by sophorose does not occur. Nonetheless, even if we must also point out the appearance of a new band at about ν= 820 cm^{-1}, though of different intensity, in both two-step samples, and a peak at 770 cm^{-1} in the 1S-80C sample, we are unable to draw any conclusion due to the lack of their clear attribution. In particular, the glucopyranose ring breathing vibration of adsorbed sophorose could be related to the peak at 770 cm^{-1}, as suggested for the adsorption of different polysaccharides on hematite,[30] but unfortunately its absence in the pure SL spectrum does not allow us proper comparisons.

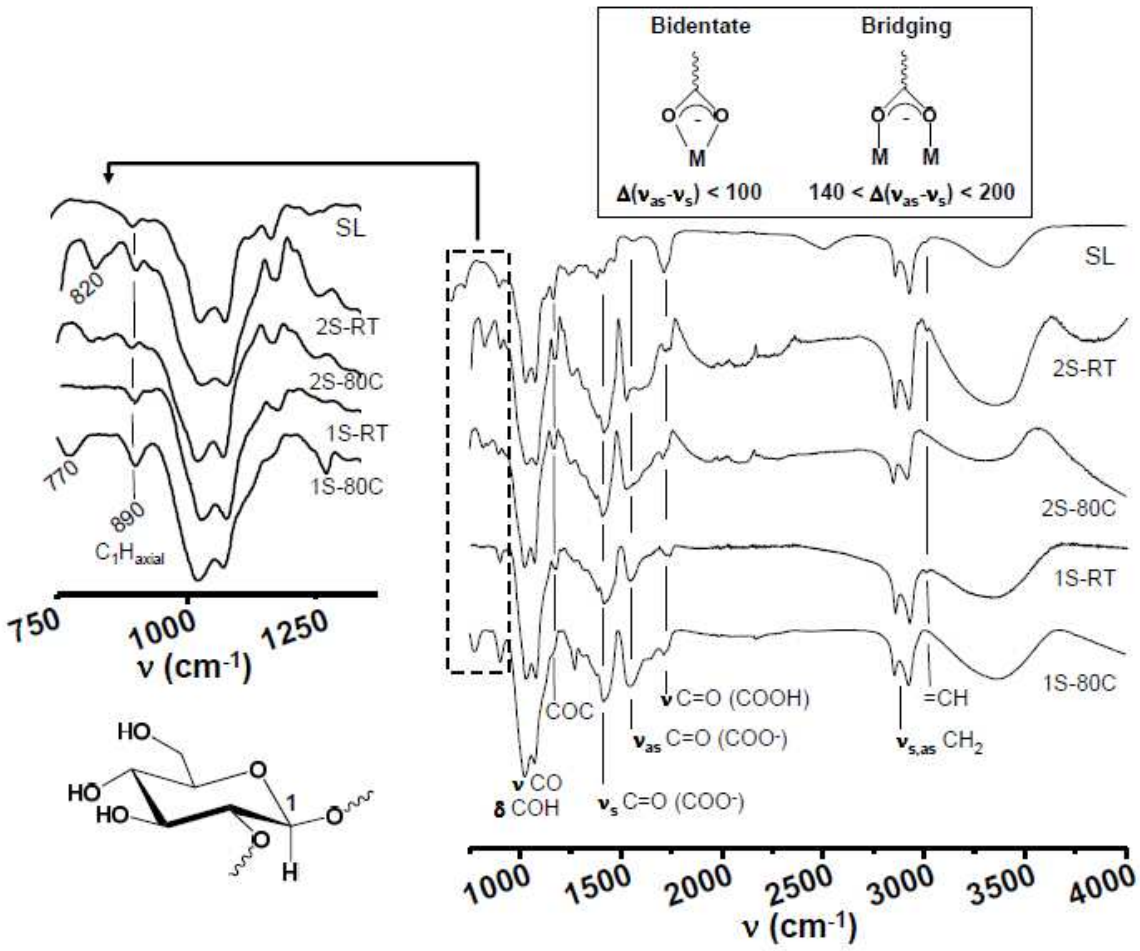

Figure 4 – FT-IR spectra of pure sophorolipid (SL) and SL-functionalized iron oxide nanoparticles. On the left, the 750 – 1250 cm^{-1} region is highlighted. The anomeric axial C_1H on the β-D-glucose (left) and the bidentate-bridging coordination modes (top, indicated values are given in cm^{-1}) are represented for sake of clarity.

According to the FT-IR analysis, it seems clear that iron oxide nanoparticles are functionalized by SL mainly via the carboxylate group and, possibly in the T= 80°C samples, by the C=C double bond of the oleic acid moiety. Nevertheless, several questions still remain open. Are SL-coated nanoparticles stable in water? Are sophorose groups readily and easily accessible at the nanoparticle surface? Previous works on this topic[14] briefly discussed the stabilization of SL-coated Ag and Co nanoparticles in water using FT-IR arguments but no specific experiments showing the stability of SL-coated particles and accessibility of sophorose were given.

The colloidal stability in water of the freshly synthesized SL-derived nanoparticles solutions strongly varies with the synthesis conditions. First of all, if no SL are employed at all, a black, water-demixed, precipitate is systematically obtained and no stable colloidal

dispersion is obtained. When SL are employed in the two-step synthesis, 2S-80C and 2S-RT samples correspond to a stable colloidal solution of maghemite nanoparticles in coexistence with a black/brown precipitate, which is probably due to nanoparticle aggregation before SL-addition and/or insufficient complexation by SL. At 80°C, the solution is clearly darker than in the experiment performed at room temperature, suggesting that either SL functionalization is more efficient, even if FT-IR experiments do not provide a clear-cut proof, or aggregation phenomena among nanoparticles before SL surface coating are reduced. Similar results are obtained on one-step experiments at room temperature while at T= 80°C, a homogeneous, monophasic, brownish stable colloidal solution is instead obtained. Citrate-derived iron oxide nanoparticles did show similar properties,[27] indicating that temperature favours seeds nucleation, whose growth is eventually limited by complexation by the COOH group of sophorolipids. All SL-derived colloidal solutions are stable over several months and centrifugation does not allow a full recover of the nanoparticles, especially for the 1S-80C system. This qualitative observation indicates the strong sophorolipid complexation effect and the steric hindrance of the sophorose group preventing particle aggregation in solution.

Particle size distribution obtained from DLS experiments in Figure 5a provide a good picture on the colloidal stability of SL-complexed nanoparticles in water, as one can see from the narrow size distribution for all samples. In Table 2, we propose a comparison between the hydrodynamic diameters, d_h (H_2O:EtOH=100:0 column), obtained from DLS and whose value is overestimated[32] with diameters previously measured by TEM, d_{TEM}, that can only be attributed to the size of the oxide particle core alone, as the electron density contrast between SL and the TEM grid support is too low to be measured correctly. According to the synthesis conditions, d_h-values for SL-coated nanoparticles range between 13 and 23 nm, which are all systematically higher than those measure by TEM, as expected. Interestingly, one can easily realize that the difference between d_h and d_{TEM} for all samples excepted the 1S-RT, whose broad size distribution in TEM did not allow a precise measurement, is actually a constant value: 10.4 ± 1.3 nm. In a previous work we estimated the radius of a spherical SL micelle to be about 3 nm,[12] which, in a first approximation, could correspond to the head-to-tail length of a single SL molecule, L_{SL}. On the contrary, the thickness of the hydration layer, L_h, of dispersed functionalized metal oxide nanoparticles in water can be evaluated by a combination of DLS, static light scattering and small angle neutron scattering experiments[33] to $1.5 < L_h < 2$ nm. The average calculated L_h[34] for our samples (1S-RT excluded) is 2.18 ± 0.64 nm, which is completely consistent with this range of values. These observations strongly supports the idea that all samples are homogeneously coated with a single

sophorolipid layer and the systematic increase of d_h values in DLS experiments can mainly be attributed to a particle core-size effect alone.

One additional method to verify the sophorose external coating of the iron oxide nanoparticles has been tested. Like all saccharides, sophorose is expected to be less soluble in low-dielectric constant solvents. This is well-known for glucose, for instance, whose solubility in ethanol is very low. At 50 mol% (76 vol%) of ethanol in water, the dielectric constant decreases from 80 to 38[35] and solubility drops from 0.4 g/mL to about 0.1 g/mL if compared to pure water.[36] According to these considerations, we expect nanoparticle aggregation phenomena to occur at a given ethanol/water mixture. The qualitative colloidal stability of the SL-coated iron oxide nanoparticles was first estimated over one week for several H_2O/EtOH mixtures and it was found that the 80/20 (vol:vol) ratio (~ 7 mol% EtOH) was a good compromise in terms of dielectric constant (~ 70)[35] and long term nanoparticle colloidal stability.[37] DLS experiments for the H_2O/EtOH=80/20 (Figure 5b) show a systematic increase of the average hydrodynamic diameter upon addition of ethanol with respect to the pure water solutions (Figure 5a). As summarized in Table 2, upon addition of ethanol to the solution, an increase between 100% and 200% in d_h is observed for samples prepared at 80°C while a ten-fold increase occurs for room temperature samples. We attribute such a large difference between RT and T= 80°C to a possible SL solubilisation effect of ethanol on more loosely bonded SL molecules at the iron oxide surface, hence inducing nanoparticle aggregations into large aggregates. Since this effect is less pronounced when synthesis temperature is set at 80°C, one could argue a more efficient surface stabilization by sophorose groups but at the moment FT-IR experiments do not support this hypothesis. Further experiments are ongoing to better understand this system.

Table 2 – Values of the hydrodynamic diameters, d_h, obtained by DLS experiments for the SL-coated iron oxide nanoparticles in water and in a 80:20 water/ethanol (vol:vol) mixture. d_{TEM} refers to the average diameters measured using TEM (Figure 3).

Sample	d_h (nm) (H_2O/EtOH=100/0)	d_h (nm) (H_2O/EtOH=80:20)	d_{TEM} (nm)
1S-RT	22.9	270.1	3-20
1S-80C	13.7	24.2	2.8
2S-RT	15.9	145.0	4.5
2S-80C	17.4	52.8	8.5

To confirm the data about the dispersive properties in water of SL-coated iron oxide nanoparticles, we have run a specific experiment where increasing amounts of a sophorolipid-free maghemite powder are redispersed in a given volume of SL-containing solution at constant concentration, C_{SL}= 0.05 g/mL. DLS diffused intensity is collected at constant shutter opening; in this case, the diffused intensity is dependent on the particle concentration. From a visual point of view, the picture shown in Figure 5c illustrates the increasing absorbed intensity of the iron oxide/SL solution as a function of the nanoparticle/SL ratio. As expected, at higher nanoparticle amount (NP/SL= 1), the solution becomes darker. In Figure 5d, the scattered intensity is reported as a function of the NP/SL ratio. These data are corrected by the solution absorption coefficient at λ= 633 nm, as presented on the right axes of Figure 5d. When the amount of nanoparticle increases, the diffused intensity increases as well, directly proving that a higher amount of nanoparticles is dispersed in the solution, thus showing the high colloidal stability of the SL-functionalized system and the stabilization effect of sophorolipids.

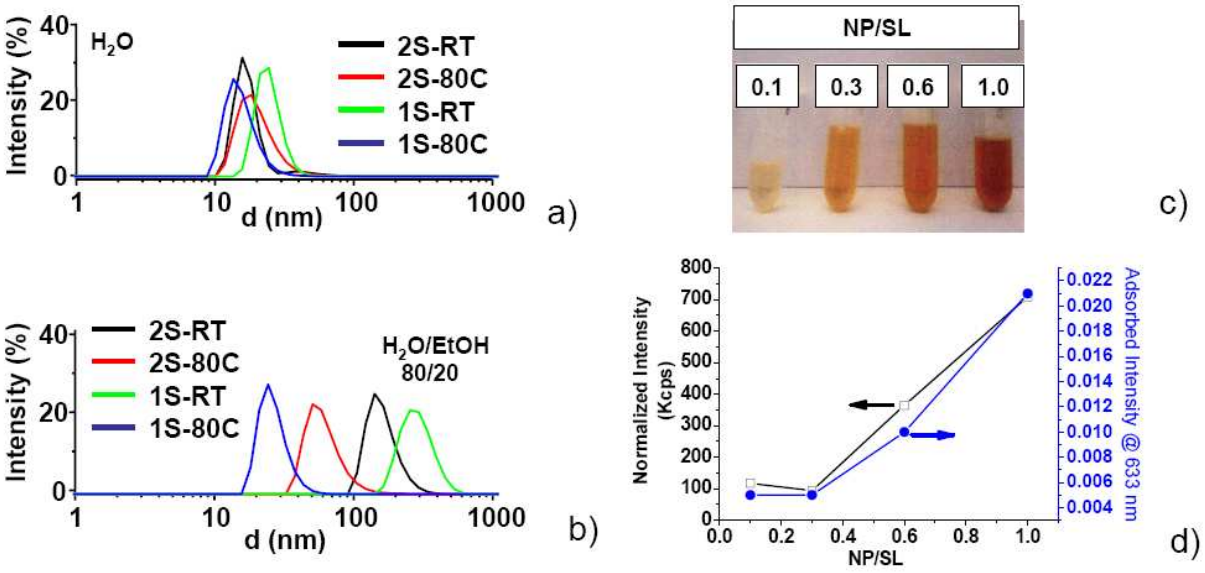

Figure 5 - a) DLS particle size distribution of all SL-functionalized iron oxide samples in water; b) DLS particle size distribution of all samples in a 80:20 = H_2O:EtOH mixture; c) images showing the concentration effect of a SL-free maghemite nanoparticles redispersed powder in a SL-containing solution at C_{SL}= 0.05 g/mL. NP/SL refers to the nanoparticle (NP) over sophorolipid (SL) mass ratio; (d) DLS diffused intensity of solutions presented in (c) in kcps (= kilocounts per second). Values are corrected for the adsorption of the same solution at λ= 633 nm and whose values are presented on the right side of the same figure. A constant shutter value of the DLS apparatus was used for these experiments.

Carbohydrate-lectin recognition.

The functionalization of iron oxide nanoparticles by glycolipids is part of an important, recent, field referred to as glyconanotechnology, where the carbohydrate moiety is used as specific interface for biocompatibility, cell interaction and molecular targeting. In particular, specific proteins, called lectins, are known to selectively bind sugars according to the affinity existing between the sugar molecular geometry and the protein cage. Lectins in general, and the specific lectin/sugar interaction, are largely studied because of their role in cell agglutination,[38] adhesion of infectious agents to host cells, recruitment of leukocytes to inflammatory sites, control of intracellular traffic of glycoproteins, cell recognition, etc... Their presence in most organisms, ranging from viruses and bacteria to plants and animals make them very important compounds in the glycobiology field and represent potential targeting sites at the surface of the concerned organism for drug delivery either within or via the organism itself.[7c]

Concanavalin A (ConA) is a plant-derived protein whose affinity towards α-D-glucopyranosyl or Q-D-mannopyranosyl sugars like D-glucose, D-fructose, D-mannose, *N*-acetyl-D-glucosamine makes it widely employed as model compound in the study of sugar/protein interactions. The C-3, C-4 and C-6 hydroxyl groups of glucose are involved in binding to the lectin and the *manno* configuration (axial hydroxyl group at C-2) has four times more affinity than the *D-gluco* configuration. Binding studies on a large number of saccharides have shown a general rule according to which ConA specifically binds non-reducing sugars with terminal α-D-glucosyl, mannosyl or *N*-acetylglucosaminyl end-groups. At pH= 7.6, ConA develops four different binding sites hence interacting with four different sugars at the same time. In particular, the specific importance and role of mannose-binding receptors has been described recently in the context of drug delivery applications.[16]

Interestingly, sophorose, a β-D-glucopyranosyl disaccharide (β–Glc-(1-2)-Glc), is not expected to have specific affinities for ConA; in reality, this was shown not to be entirely correct as a fair/medium affinity for ConA was actually observed; in particular, the free hydroxyl groups at C-3, C-4 and C-6 positions of the reducing glucose residue of the disaccharide were proposed to be the main ConA binding sites.[39] Nevertheless, one drawback of using sophorolipids is that no reducing unit is actually kept in the sophorose group because of the glycosidic bond between the C-17 of the fatty acid with the anomeric carbon of β-D-glucose. For these reasons, a specific interaction between ConA and sophorose in sophorolipids-grafted nanoparticles is uncertain.

In Figure 6 we present the adsorption of two different lectins, ConA and Lectin from *Bandeiraea simplicifolia* (BS-I) on SL-functionalized magnetic nanoparticles. The sample 2S-80C is selected for its magnetic properties, which allow to filter it out of the solution rather easily using an external magnet. While the interaction between ConA and sophorose has been specifically studied, no reports are available describing the interaction between sophorose and Lectin from *Bandeiraea simplicifolia*, whose known affinity is mainly towards *N*-acetyl-D-glucosamine.[40] At this stage, we expect no specific binding affinity between BS-I and sophorose. Additionally, specific interactions between lectins and non-functionalized iron oxide nanoparticles are not expected either, as proved by El-Boubbou et al.[6a] Adsorption studies between ConA-FITC, BS-I-FITC and SL-grafted nanoparticles are shown in Figure 6. The FITC-conjugation on both proteins allows their direct detection in solution by fluorescence emission spectroscopy at λ= 565 nm (excitation wavelength, λ_{ex}= 494 nm). Red and green spectra refer to two specific protein concentration values in solution at pH= 7.4 used as reference: 0.125 and 0.025 mg/mL for BS-I and 0.01 and 0.05 mg/mL for ConA. The 2S-80C SL-nanoparticle sample was introduced in the highest lectin concentration solution and let under mechanical agitation for 1 hour at room temperature. Concentration of residual FITC-lectins in solution is measured spectrophotometrically after particle filtering using an external magnet. When BS-I is used (c= 0.125 mg/mL), there is no variation in the FITC emission spectrum before and after adding the nanoparticles at three different concentrations, indicating that no specific interaction occurs between BS-I and sophorose (Figure 6b). On the contrary, the same experiment performed with ConA (initial concentration, c= 0.05 mg/mL) shows a 65% decrease in the FITC emission intensity upon addition of 0.5 mg/mL of 2S-80C (black spectrum), as shown in Figure 6a. At lower nanoparticles concentration values, 0.25 and 0.05 mg/mL, the decrease in FITC emission is, respectively, 52% (blue spectrum) and 41% (cyan spectrum) indicating that the amount of remaining FITC-conjugated ConA in solution is higher, due to the lower amount of supported sophorose groups, as one would expect. Overall, lectin adsorption does not vary with increasing mixing time (concentration tests were repeated after 3 hours and one night stirring). The conditions employed to reach the 65% intensity reduction (black spectrum) are comparable with the system presented by El-Boubbou et al.[6a] These authors have shown that the use of mannose, the sugar having the highest affinity known for ConA, in mannose-conjugated iron oxide nanoparticles is responsible for the reduction of 89% of the FITC signal due to mannose-ConA specific affinity. This shows that sophorose, despite the expected low affinity for ConA, is nonetheless able to compete with mannose-derived particles.

In the perspective of potential use of sophorolipids in bio-glyconanotechnology applications, this result is extremely interesting.

- These experiments prove that sophorolipids can be directly grafted in a stable manner onto iron oxide nanoparticles through their COOH group keeping the sophorose accessible on the outer shell of the particle. The presence of the sophorose makes nanoparticles both non-toxic, biocompatible and of potential use in biotargeting applications.
- Sophorolipids can be used as selective targets for sugar-binding proteins exhibiting an affinity for sophorose. To the best of our knowledge, the specific affinity of lectins for sophorose constitutes a new field of research, as literature data on this topic as scarcely available.
- Sophorolipids are interesting compounds that can be tested as selective targets even for non-sophorose binding proteins, as shown by the results obtained on ConA and BS-I. Both proteins are known not to have a specific affinity for sophorose, even if ConA was reported once in a long-dated work[39] to exhibit a moderate affinity for the reducing moiety of this specific disaccharide. Here we demonstrate that selectivity (BS-I versus ConA) is still valid, but at the same time full affinity does not need to be matched in order to exploit sophorolipids in lectin targeting applications. In this context, sophorolipids, easy-to-obtain natural glycoconjugates, could replace mannose functionalization in targeting applications of specific organs like liver and kidneys or macrophages and monocytes, in the case that mannose receptors at the organism's surface[16,41] also show a specific affinity for sophorose.

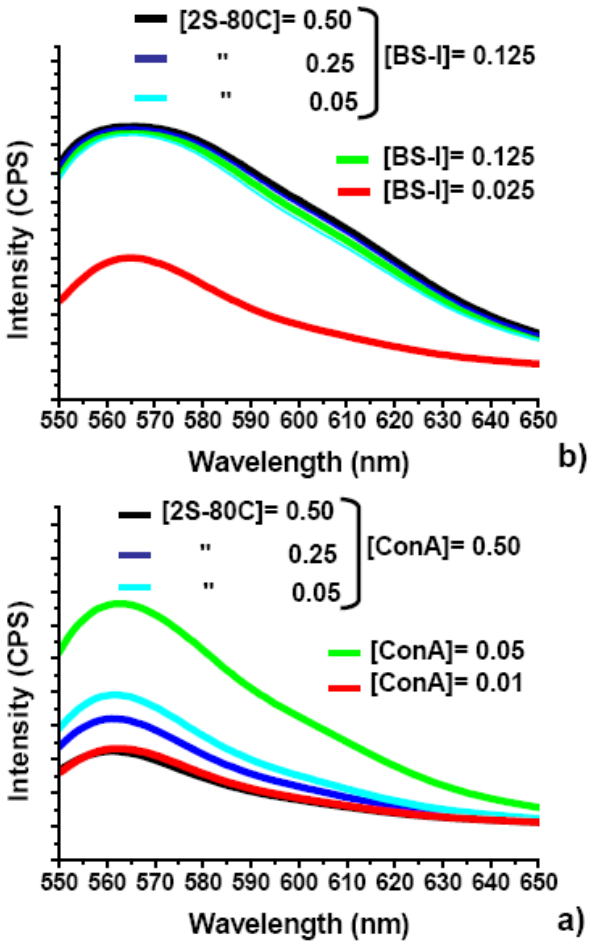

Figure 6 – Fluorescence emission spectra of FITC-grafted a) ConA and b) BS-I with and without addition of SL-grafted magnetic iron oxide nanoparticles (2S-80C sample). Red and green spectra refer to blank reference lectin solutions while black, cyan and blue spectra refer to lectin/nanoparticles mixed systems at various concentrations of nanoparticles. All values are given in mg/mL.

Conclusion

The use of biosurfactants in non-deterging, material science related, applications is a recent research field that takes into account the astonishing and multivalent, yet unknown, properties of some of these compounds. In this work, we have used the acidic form of sophorolipids, a glycolipid containing a sophorose head covalently bonded to an oleic acid moiety, to functionalize magnetic iron oxide nanoparticles, a material which is largely studied for bionanotechnology applications like MRI contrast agent and hyperthermia. The multi-compound functionalization approach which is commonly followed to tune the surface properties of iron oxide nanoparticles (e.g., use of surfactants, polymers and biomolecules are combined to provide water solubility, stealth and cell-targeting properties) is replaced here by employing a multivalent glyconjugate. Glycolipids are more and more tested as nanoparticle coating agents because of their multiple advantages like enhanced hydrophilicity, biocompatibility and protein-recognition properties making them attractive compounds for

biomedical applications. In general, these compounds are synthesized using multiple chemical steps and the molecular design is done according to the desired final application. In this work, we have shown that a given glycolipid of entirely natural origin can be adapted as surface functional agent. The use of sophorolipids in either one-step or two-steps synthesis procedure of iron oxide nanoparticles shows a strong effect on the final material's structure. In particular, in one-step synthesis poorly crystalline ferrihydrite nanoparticles are obtained instead of magnetite (or maghemite) ones, indicating the complexation effect of the COOH group on iron metal centers during synthesis. The two-step approach provides classical γ-Fe_2O_3 nanoparticles. Whatever the synthesis protocol, all synthesis FT-IR experiments show that sophorolipids interact with the iron oxide surface via their carboxylic group imprinting a large colloidal stability to the final material, as also shown by TEM and DLS experiments. No interactions between sophorose and iron were observed according to FT-IR axperiments. In addition, according to DLS data, the amount of dispersed nanoparticles in solution increases with increasing nanoparticle/sophorolipid mass ratio. The accessibility of the sophorose group at the surface of the nanoparticle is also an important issue. First of all, we have shown that changing the dielectric constant of the dispersing medium causes aggregation of the nanoparticles, as expected for sugar-coated compounds. Most importantly, we proved the accessibility of the sophorose group by playing with selective sugar/protein affinities. A specific family of proteins, called lectins, have the ability to selectively bind mono and polysaccharides. Here, through fluorescence emission spectrum, we have shown that the sophorose unit of the sophorolipid molecule selectively binds Concanavalin A (ConA, a mannose-binding lectin) with respect to Lectin from *Bandeiraea simplicifolia* (BS-I, a *N*-acetyl-D-glucosamine binding lectin), both FITC-conjugated. This result is extremely important beyond the accessibility of sophorose at the nanoparticle's surface. The affinity of sophorose for lectins is poorly studied and here, such an affinity was not expected because sophorose has non-reducing properties in sophorolipids. For this, the good affinity of ConA for sophorolipids (65% of FITC-ConA signal reduction compared to 89% obtained on mannose-derived system under comparable conditions[6a]), in combination with the lack of sophorose/BS-I binding, address the important issue of possible use of sophorolipids-complexed materials in targeting applications and, in particular, as possible replacement for mannose-functionalized nanoobjects.

Acknowledgements

The research leading to these results has received funding from the European Community's Seventh Framework Programme (FP7/2007-2013) under Grant Agreement n° Biosurfing/289219. The authors thank Dr. Moulay-Tahar Sougrati (Institut Charles Gerhardt, Montpellier) for the preparation of the Mössbauer absorbers and the recording of Mössbauer spectra and Patrick Le Griel (Laboratoire de Chimie de la Matière Condensée de Paris, Paris, France) for kind assistance on TEM experiments. Jerôme Fresnais (Physicochimie des Electrolytes, Colloïdes et Sciences Analytiques, Paris, France) is kindly acknowledged for helpful discussions on DLS experiments and Marie Guerard (Ecole Nationale Supérieure de Chimie Rennes, Rennes, France) for her involvement in some synthesis work.

References

[1] R. Bardhan, S. Lal, A. Joshi, N. J. Halas, *Acc. Chem. Res*., **2011**, 44, 936-946
[2] a) C. Fang, M. Zhang, *J. Mater. Chem*., **2009**, 19, 6258-6266; b) J. Xie, G. Liu, H. S. Eden, H. Ai, X. Chen, Acc. Chem. Res., 2011, 44, 883-892; c) F. M. Kievit, M. Zhang, *Acc. Chem. Res*., **2011**, 44, 853-862
[3] S. Laurent, D. Forge, M. Port, A. Roch, C. Robic, L. Vander Elst, R. N. Muller, *Chem. Rev*., **2008**, 108, 2064–2110
[4] a) C. Fang, M. Zhang, *J. Mater. Chem*., **2009**, 19, 6258-6266; b) J. Xie, G. Liu, H. S. Eden, H. Ai, X. Chen, Acc. Chem. Res., 2011, 44, 883-892; c) F. M. Kievit, M. Zhang, *Acc. Chem. Re*s., **2011**, 44, 853-862
[5] F. M. Kievit, M. Zhang, *Acc. Chem. Res*., **2011**, 44, 853-862
[6] a) K. El-Boubbou, D. C. Zhu, C. Vasileiou, B. Borhan, D. Prosperi, W. Li, X. Huang, *J. Am. Chem. Soc*., **2010**, 132, 4490–4499; b) A. G. Barrientos, J. M. de la Fuente, T. C. Rojas, A. Fernandez, S. Penades, *Chem. Eur. J*., **2003**, 9, 1909-1921; c) C. Earhart, N. R. Jana, N. Erathodiyil, J. Y. Ying, *Langmuir*, **2008**, 24, 6215-6219; d) B. K. Gorityala, J. Ma, X. Wang, P. Chen, X.-W. Liu, *Chem. Soc. Rev*., **2010**, 39, 2925–2934
[7] a) Y. C. Lee, R. T. Lee, *Acc. Chem. Res*., **1995**, 28, 321-327; b) T. Buskas, P. Thompson, G.-J. Boons, *Chem. Commun*., **2009**, 5335–5349; c) H. Lis, N. Sharon, *Chem. Rev*., **1998**, 98, 637-674; d) P. H. Seeberger, D. B. Werz, *Nature*, **2007**, 446, 1046-1051
[8] a) C. Earhart, N. R. Jana, N. Erathodiyil, J. Y. Ying, *Langmuir*, **2008**, 24, 6215-6219; b) F. Santoyo-Gonzalez, F. Hernandez-Mateo, *Chem. Soc. Rev*., **2009**, 38, 3449-3462
[9] D. W. G. Develter, L. M. L. Lauryssen, *Eur. J. Lipid Sci. Technol*., **2010**, 112, 628–638
[10] a) M. Maingault, Use of sophorolipids and cosmetic and dermatological compositions, WO/1995/034282A; b) I. N. A. Van Bogaert, K. Saerens, C. De Muynck, D. Develter, W. Soetaert, E. J. Vandamme, *Appl. Microbiol. Biotechnol.*, **2007**, 76, 23‑34; c) A. M. Shete, G. Wadhawa, I. M. Banat, B. A. Chopade, *J. Sci. Ind. Res*., **2006**, 65, 91-11
[11] S. L. Fu, S. R. Wallner, W. B. Bowne, M. D. Hagler, M. E. Zenilman, R. Gross, M. H. Bluth, *J. Surg. Res*., **2008**, 148, 77-82
[12] N. Baccile, N. Nassif, L. Malfatti, I. N. A. Van Bogaert, W. Soetaert, G. Pehau-Arnaudetd, F. Babonneau, *Green Chem*., **2010**, 12, 1564–1567
[13] S. Zhou, C. Xu, J. Wang, W. Gao, R. Akhverdiyeva, V. Shah, R. Gross, *Langmuir*, **2004**, 20, 7926-7932
[14] a) S. Singh, P. Patel, S. Jaiswal, A. A. Prabhune,C. V. Ramana, B. L. V. Prasad, *New J. Chem*., **2009**, 33, 646–652; b) M. Kasture, S. Singh, P. Patel, P. A. Joy, A. A. Prabhune, C. V. Ramana, B. L. V. Prasad, *Langmuir* **2007**, 23, 11409-11412
[15] S. Dhar, E. M. Reddy, A. Prabhune, V. Pokharkar, A. Shiras, B. L. V. Prasad, *Nanoscale*, **2011**, 3, 575–580
[16] J. M. Irache, H. H. Salman, C. Gamazo, S. Espuelas, *Exp. Op. Drug Deliv.*, **2008**, 5, 703-724
[17] S. Lang, A. Brakemeier, R. Heckmann, S. Spockner, U. Rau, *Chim Oggi-Chem Today*, **2000**, 18, 76-79
[18] U. Rau, R. Heckmann, V. Wray, S. Lang, *Biotechnol. Lett*., **1999**, 21, 973-977
[19] a) R. Massart, *IEEE Trans. Magn*., **1981**, 17, 1247; b) R. Massart, V. Cabuil, *J. Chim. Phys*., **1987**, 84, 7

[20] a) J. Park, L. H. Rader, G. B. Thomas, E. J. Danoff, D. S. English, P. DeShong, *Soft Matter*, **2008**, 4, 1916-1921; b) C.-C. Lin, Y.-C. Yeh, C.-Y. Yang, G.-F. Chen, Y.-C. Chen, Y.-C. Wu, C.-C. Chen, *Chem. Commun*., **2003**, 2920-2921

[21] G. Grosse, PC-Mos II; 1.0 ed.; Technische Universität München Munich (Germany), 1993.

[22] J. L. Jambor, J. E. Dutrizac, *Chem. Rev*., **1998**, 98, 2549-2585

[23] G. M. da Costa, E. De Grave, P. M. A. de Bakker, R. E. Vandenberghe, *J. Solid State Chem*., **1994**, 113, 405-412

[24] R. M. Cornell, U. Schwertmann, *The Iron Oxides*, Ed VCH Weinheim, 1996

[25] L. Babes, B. Denizot, G. Tanguy, J. J. Le Jeune, P. Jallet, *J. Colloid Interf. Sci*., **1999**, 212, 474–482

[26] a) K. Kandori, M. Fukuoka, T. Ishikawa, *J. Mater. Sci*., **1991**, 26, 3313-3319; b) G. S. R. Krishnamurti, P. M. Huang, *Clays Clay Miner*., **1991**, 39, 28-34

[27] A. Bee, R. Massart, S. Neveu, *J. Magn. Magn. Mater*., **1995**, 149, 6-9

[28] a)Bala, T.; Swami, A.; Prasad, B. L. V.; Sastry, M. *J. Colloid Interface. Sci.*, **2005**, 283, 422 ; b) Wang, W.; Efrima, S.; Regev, O. *Langmuir*, **1998**, 14, 602

[29] a) Y. Lu, J. D. Miller, *J. Coll. Interf. Sci*., **2002**, 256, 41–52; b) L. M. Bronstein, X. Huang, J. Retrum, A. Schmucker, M. Pink, B. D. Stein, B. Dragnea, *Chem. Mater*. **2007**, 19, 3624-3632; c) Nakamoto, K. Infrared and Raman Spectra of Inorganic and Coordination Compounds, Part B: Applications in Coordination, organometallic and Bioinorganic Chemistry, 5th ed., Wiley: New York, 1997, p 387

[30] P. K. Weissenborn, L. J. Warren, J. G. Dunn, *Coll. Surf. A*, **1995**, 99, 27

[31] J. Blackwell, P. D. Vasko, J. L. Koenig, *J. Appl. Phys*., 1970, 41, 4375

[32] DLS overestimates the value of the nanoparticle diameter; for this reason it is referred here to as hydrodynamic diameter, d_h, which is inversely proportional to the medium viscosity and diffusion coefficient according to the Stokes equation.

[33] L. Qi, A. Sehgal, J.-C. Castaing, J.-P. Chapel, J. Fresnais, J.-F. Berret, F. Cousin, *ACS Nano*, **2008**, 2, 879–888

[34] This value is estimated by considering the difference between the hydrodynamic radius ($d_h/2$) in water, the head-to-tail distance of SL (3 nm) and the nanoparticle core diameter ($d_{TEM}/2$): L_h [nm]= $d_h/2$ - 3 - $d_{TEM}/2$, where d_h and d_{TEM} values are given in Table 2.

[35] H. Yilmaz, *Turk. J. Phys*., **2002**, 26, 243-246

[36] L. A. Alves, J. B. Almeida e Silva, M. Giulietti, *J. Chem. Eng. Data*, **2007**, 52, 2166-2170

[37] No macroscopic nanoparticle aggregation phenomena were observed for over one month after dilution

[38] Cell agglutination refers to the ability of lectins to bind sugar moieties at cell surfaces allowing cell-cell interaction and their precipitation.

[39] a) J. Goldstein, R. N. Iyer, E. E. Smith, L. L. So, *Biochem*., **1967**, 6, 2373-2377; b) J. Montreuil, J. F. G. Vliegenthart, H. Schachter, Glycoproteins II, 1997, Vol. 29, Part 2, Chapter 14, Elsevier

[40] C. E. Hayes, I. J. Goldstein, *J. Biol. Chem*., **1974**, 249, 1904-1914

[41] A. Nag, P. C. Gosh, *J. Drug Target*., **1999**, 6, 427-438